Publication Year	2020
Acceptance in OA@INAF	2023-01-16T16:52:51Z
Title	A dusty benchmark brown dwarf near the ice line of HD 72946
Authors	Maire, A. -L.; Baudino, J. -L.; Desidera, S.; MESSINA, Sergio; Brandner, W.; et al.
DOI	10.1051/0004-6361/201937134
Handle	http://hdl.handle.net/20.500.12386/32881
Journal	ASTRONOMY & ASTROPHYSICS
Number	633

Astronomy & Astrophysics manuscript no. ms
December 10, 2019

Letter to the Editor

A dusty benchmark brown dwarf near the ice line of HD 72946★

A.-L. Maire[1, ★★], J.-L. Baudino[2], S. Desidera[3], S. Messina[4], W. Brandner[5], N. Godoy[6, 7], F. Cantalloube[5], R. Galicher[8], M. Bonnefoy[9], J. Hagelberg[10], J. Olofsson[6, 7], O. Absil[1, ★★★], G. Chauvin[9, 11], T. Henning[5], and M. Langlois[12]

(Affiliations can be found after the references)

Received 18 November 2019 / Accepted 4 December 2019

ABSTRACT

Context. HD 72946 is a bright and nearby solar-type star hosting a low-mass companion at long period ($P \sim 16$ yr) detected with the radial velocity (RV) method. The companion has a minimum mass of 60.4±2.2 M_J and might be a brown dwarf. Its expected semi-major axis of ~243 mas makes it a suitable target for further characterization with high-contrast imaging, in particular to measure its inclination, mass, and spectrum and thus definitely establish its substellar nature.

Aims. We aim to further characterize the orbit, atmosphere, and physical nature of HD 72946B.

Methods. We present high-contrast imaging data in the near-infrared with the Spectro-Polarimetric High-contrast Exoplanet REsearch (SPHERE) instrument. We also use proper motion measurements of the star from Hipparcos and *Gaia*.

Results. The SPHERE data reveal a point source with a contrast of ~9 mag at a projected separation of ~235 mas. No other point sources are detected in the field of view. By jointly fitting the RV, imaging, and proper motion data, we constrain all the orbital parameters of HD 72946B and assess a dynamical mass of 72.4±1.6 M_J and a semi-major axis of $6.45^{+0.08}_{-0.07}$ au. Empirical comparison of its SPHERE spectrum to template dwarfs indicates a spectral type of L5.0±1.5. The J-$H3$ color is close to the expectations of the DUSTY models and suggests a cloudy atmosphere. Comparison with atmospheric models of the spectrophotometry suggests an effective temperature of ~1700 K. The bolometric luminosity ($\log(L/L_\odot)$ = -4.11±0.10 dex) and dynamical mass of HD 72946B are more compatible with evolutionary models for an age range of ~0.9–3 Gyr. The formation mechanism of the companion is currently unclear as the object appears slightly away from the bulk of model predictions. HD 72946B is currently the closest benchmark brown dwarf companion to a solar-type star with imaging, RV, and proper motion measurements.

Key words. brown dwarfs – methods: data analysis – stars: individual: HD 72946 – planet and satellites: dynamical evolution and stability – techniques: high angular resolution – techniques: image processing

1. Introduction

Dynamical mass measurements of brown dwarfs are a powerful test of their formation and evolution models. Most studies exploit brown dwarf binaries (e.g., Konopacky et al. 2010; Dupuy & Liu 2017; Dieterich et al. 2018), which have likely formed by fragmentation of a collapsing cloud (e.g., Bate 2009). However, it is still unclear whether brown dwarfs found at close-in separations to stars form like stellar binaries or by disk gravitational instabilities (Boss 1997). In the past years, a few radial velocity (RV) surveys started to target stars with slow drifts to constrain the orbit and minimum mass of the suspected long-period companions (e.g., Bouchy et al. 2016; Sahlmann et al. 2011; Feroz et al. 2011). These surveys have shown a paucity of brown dwarf companions within 5 au from the host stars with respect to planetary and stellar companions (the so-called "brown dwarf desert", see e.g., Grether & Lineweaver 2006; Sahlmann et al. 2011; Ma & Ge 2014). Nevertheless, Ma & Ge (2014) found that their occurrence increases at larger separations when brown dwarf detections from various techniques are combined.

Using the ELODIE and SOPHIE instruments, Bouchy et al. (2016) reported a potential brown dwarf companion to the G5V star HD 72946, located at 25.87±0.08 pc (Gaia Collaboration et al. 2016, 2018). The RV data cover a full orbit of HD 72946B, which allowed the authors to place good constraints on its orbit (period $P = 15.93^{+0.15}_{-0.13}$ yr, eccentricity $e = 0.495 \pm 0.006$, and periastron T_0 [HJD] $= 2455958 \pm 10$). They derived a minimum dynamical mass of 60.4±2.2 M_J and an upper mass limit of 0.2 $M_\odot$ from the analysis of the cross-correlation function of the star.

We present in this paper the confirmation and characterization of the brown dwarf companion to HD 72946 with the Spectro-Polarimetric High-contrast Exoplanet REsearch (SPHERE) instrument and Hipparcos-*Gaia* proper motion measurements. We present an updated analysis of the properties of the host star in Sect. 2 and the SPHERE imaging observations in Sect. 3. We perform a joint orbital fit of the imaging, RV, and astrometric data and derive a dynamical mass for HD 72946B in Sect. 4. Section 5 discusses the spectral properties of the companion. Finally, we compare the physical and spectral properties of HD 72946B to model predictions in Sect. 6.

2. Properties of the host star

Bouchy et al. (2016) inferred from spectroscopic observations an effective temperature $T_{\rm eff}$ = 5686± 40 K, a surface gravity $\log g = 4.50 \pm 0.06$ dex, and a metallicity [Fe/H] = 0.11±0.03 dex. The supersolar metallicity has been confirmed by other studies (Aguilera-Gómez et al. 2018; Luck & Heiter 2006; Casagrande et al. 2011, 0.15±0.06, 0.16±0.04, and 0.12 dex, respectively).

We derived the stellar age and mass from isochrones using the PARAM web interface[1] (da Silva et al. 2006). We adopted

---

★ Based on observations collected at the European Organisation for Astronomical Research in the Southern Hemisphere under ESO programme 0102.C-0781.

★★ F.R.S.-FNRS Postdoctoral Researcher.

★★★ F.R.S.-FNRS Research Associate.

[1] http://stev.oapd.inaf.it/cgi-bin/param_1.3

Table 1. Relative photometry and astrometry of HD 72946B.

Filter	λ_0 (µm)	$\Delta\lambda$ (µm)	Δmag (mag)	Abs. mag. (mag)	Flux ($\times 10^{-15}$ W m^{-2} µm^{-1})	Separation (mas)	PA (°)
*H*2	1.593	0.052	8.97±0.07	12.51±0.07	3.027±0.188	235.7±2.0	33.65±0.31
*H*3	1.667	0.054	8.81±0.07	12.35±0.07	3.236±0.204	235.6±2.0	33.68±0.31

Notes. The photometric error bars were derived assuming an error budget including the measurement uncertainties (image post-processing) and systematic uncertainties (temporal variability of the flux calibration and of the science sequence).

the spectroscopic $T_{\rm eff}$ and [Fe/H] in Bouchy et al. (2016) with enlarged uncertainties to account for systematic errors. We also adopted the *Gaia* parallax and the *V*-band magnitude from Hipparcos (7.08±0.02 mag). This results in an age 1.712±1.684 Gyr, a mass 0.986±0.027 $M_\odot$, and a radius 0.908±0.018 $R_\odot$. Tighter constraints on the age from isochrones can be derived from the F8 comoving companion HD 72945 (1.6±1.0 Gyr, Appendix A).

Lithium data (A(Li) = 1.41, 1.23, 1.22±0.15 dex, Luck 2017; Luck & Heiter 2006; Ramírez et al. 2012) indicate an age older than that of the Hyades and similar to the open cluster NGC 752 (Sestito et al. 2004). The stellar kinematics suggest an age younger than the Sun, the UVW velocities being at the boundary of the kinematic space of young stars in Montes et al. (2001). Comparisons with stars with similar kinematics in Casagrande et al. (2011) indicated that it is unlikely that the star is older than ~3 Gyr and much younger than 0.5 Gyr.

We searched for archival photometric data to derive an age with gyrochronology, but we did not find suitable data (sampling, accuracy, blending with HD 72945, and/or calibration issues). Using the relations in Mamajek & Hillenbrand (2008) and an averaged measured chromospheric activity of -4.60 dex (individual values -4.54, -4.74±0.05, -4.66, and -4.47 dex, Rocha-Pinto et al. 2004; Bouchy et al. 2016; Gray et al. 2003; Boro Saikia et al. 2018), we derive a rotation period of ~15 d, which implies a gyrochronological age of ~1 Gyr. This is in between the loci of the Hyades (625–700 Myr) and NGC 752 (2000 Myr). The star has X-ray data from ROSAT, but is blended with HD 72945. However, X-ray activity is expected to correlate with chromospheric activity, so that it does not provide a fully independent age estimate. Assuming our derived stellar radius and an averaged measured projected rotational activity of 4.14 km s^{-1} (individual values 3.23, 3.9±1, and 5.3 km s^{-1}, Martínez-Arnáiz et al. 2010; Bouchy et al. 2016; Luck 2017), we derive an upper limit for the rotation period of 12 d, which implies a gyrochronological age younger than 1 Gyr considering a $B-V$ color of 0.71 mag. Considering the large uncertainties in $v \sin i_\star$, the upper limit for the gyrochronological age could be as old as 1.5 Gyr. This means that our various age estimates agree overall. In the following, we choose to adopt an age range of 0.8–3 Gyr, with a most probable value of 1–2 Gyr.

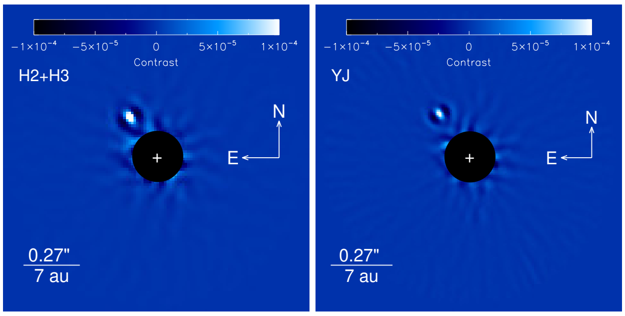

Fig. 1. SPHERE contrast images of HD 72946. The central regions of the images are numerically masked out to hide bright stellar residuals. The white crosses indicate the location of the primary star.

3. Observations and data analysis

We observed HD 72946 on 2019 March 21 UT with the standard IRDIFS mode of SPHERE (Beuzit et al. 2019), which allows for simultaneous near-IR observations with IRDIS with the *H*23 filter pair (Dohlen et al. 2008; Vigan et al. 2010) and the integral field spectrograph IFS in the *YJ* bands (Claudi et al. 2008). The seeing and coherence time measured by the differential image motion monitor at 0.5 µm were 0.5–0.7″ and 6-8 ms, respectively. The detector integration time was set to 16 s, and 128 frames were recorded, amounting to a field rotation of 15.5°.

An apodized pupil Lyot coronagraph (Carbillet et al. 2011; Martinez et al. 2009) was used. We acquired data before and after the sequence to calibrate the flux of the images and the location of the star behind the coronagraph (Langlois et al. 2013). Nighttime sky background frames were taken and additional daytime calibration performed following the standard procedure at ESO.

The data were reduced with the SPHERE Data Reduction and Handling software (v0.15.0, Pavlov et al. 2008) and custom routines for IFS data adapted from Mesa et al. (2015) and Vigan et al. (2015). This corrected for the cosmetics and instrument distortion, registered the frames, and normalized their flux. For IFS, it also performed the wavelength calibration and extracted the image cubes. Then, the data were analyzed with angular differential imaging (Marois et al. 2006) using three algorithms (Appendix B): ANDROMEDA, TLOCI, and PCA. Figure 1 shows the ANDROMEDA images.

The photometry and astrometry were extracted using three algorithms, but we chose to retain the TLOCI values (Table 1). The astrometry was calibrated following Maire et al. (2016), with pixel scales of 12.255±0.009 mas/pix (*H*2) and 12.251±0.009 mas/pix (*H*3) and a North correction angle of −1.75±0.08°. The absolute magnitudes were computed using the 2MASS values (Cutri et al. 2003) for the stellar magnitudes.

4. Orbital analysis

We retrieved the RV measurements in Bouchy et al. (2016) through the VizieR interface. With only one imaging data point, there is still an ambiguity in the inclination and longitude of the ascending node. To solve for this, we also searched for an astrometric signature of the companion in the Hipparcos-*Gaia* catalog of accelerations (Brandt 2018, 2019): pmra_g_hg = −2.837±0.140 mas yr^{-1} and pmdec_g_hg

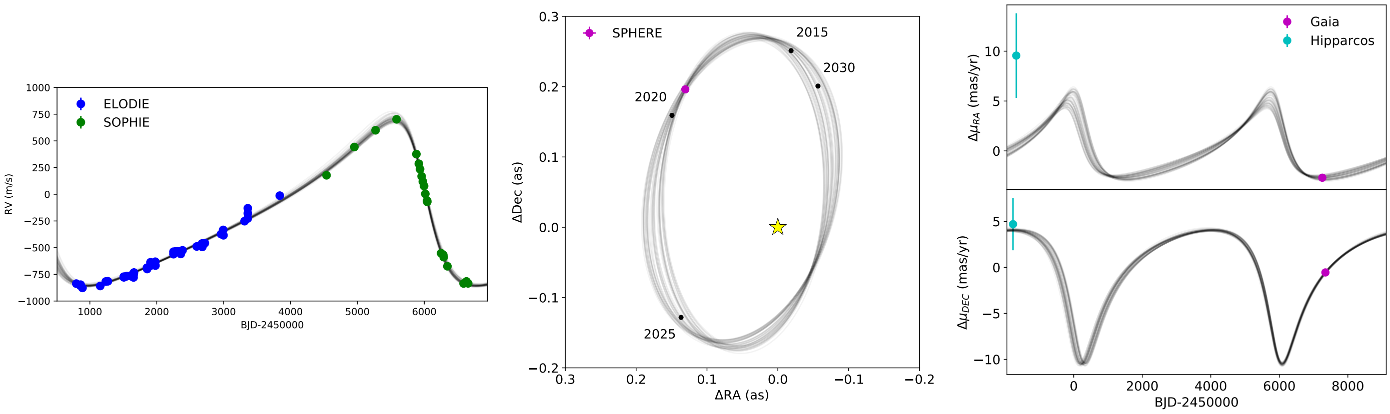

Fig. 2. Sample of 50 model orbits fitted on the HD 72946B data (colored points) from RV (*left*), imaging (*middle*), and astrometry (*right*). In the *middle* panel, the yellow star marks the location of the primary star, and the black dots show the median predicted position for given epochs.

= −0.515±0.082 mas yr^{-1} for *Gaia* (Gaia Collaboration et al. 2018), pmra_h_hg = 9.411±4.245 mas yr^{-1} and pmdec_h_hg = 4.734±2.839 mas yr^{-1} for Hipparcos (Perryman et al. 1997; van Leeuwen 2007). These values imply an astrometric detection at (20.3, 6.3)σ with *Gaia* and (2.1, 1.7)σ with Hipparcos. We verified that the *Gaia* DR2 record is well behaved, with a renormalized unit weight error below 1.4 (Lindegren et al. 2018).

We performed a joint fit of the RV, imaging, and proper motion data with the parallel-tempered Markov chain Monte Carlo (MCMC) algorithm provided in the `emcee` package (Foreman-Mackey et al. 2013), which is based on the algorithm described by Earl & Deem (2005). Our implementation follows Brandt et al. (2019a) in the broad lines. We sampled the parameter space of our 13-parameter model assuming 15 temperatures for the chains and 100 walkers. The first 8 parameters are the semi-major axis a, the eccentricity e and argument of periastron passage ω (parameterized as $\sqrt{e}\cos\omega$ and $\sqrt{e}\sin\omega$), the inclination i, the longitude of the ascending node Ω, the time at periastron passage T_0, the RV semi-amplitude of the star κ_A, and the systemic velocity γ. We present the results for Ω and ω as relative to the companion. To fit the imaging and proper motion data, we used the equations in Appendix A of Makarov & Kaplan (2005).

The initial state of the sampler was set assuming uniform priors in $\log a$, $\sqrt{e}\cos\omega$, $\sqrt{e}\sin\omega$, Ω, T_0, and κ_A, as well as a $\sin i$ prior for i. The width of the priors were selected from the results in Bouchy et al. (2016) and a fit to the RV and imaging data with a least-squares Monte Carlo approach (Maire et al. 2015; Schlieder et al. 2016) to derive first ranges for i and Ω. We disentangled the two (i,Ω) solutions by comparing the predictions for the instantaneous stellar proper motions to the measurements.

The next two parameters in our model are the parallax and the semi-major axis of the orbit of the host star around the center of mass of the system. For the parallax, we drew the initial guesses around the nominal value measured by *Gaia* assuming a combination of a Gaussian distribution for the measurement uncertainties and a uniform distribution for potential systematics (<0.1 mas, https://www.cosmos.esa.int/web/gaia/dr2). We drew the semi-major axis of the star around a guess value computed from its mass (0.99 $M_\odot$), the companion mass (0.07 $M_\odot$), and the total semi-major axis, assuming a uniform distribution with a half-width of 1.5 mas. The last free model parameters are one RV offset and two RV jitters, using the results in Bouchy et al. (2016) as first guesses.

We ran the MCMC for 125 000 iterations and verified the convergence of the chains using the integrated autocorrelation time (Foreman-Mackey et al. 2013; Goodman & Weare 2010). The posterior distributions in Appendix C were obtained after thinning the chains by a factor 100 to mitigate the correlations and discarding the first 75% of the chains as the burn-in phase. The median values with 1σ uncertainties and the best-fit values of the parameters are given in Table 2. The uncertainties in the parameters in common with Bouchy et al. (2016) are slightly larger or similar. A sample of model orbits is shown in Fig. 2.

Table 2. Orbital parameters and dynamical mass of HD 72946B.

Parameter	Unit	Median ± 1σ	Best fit
Fitted parameters			
Semi-major axis a	mas	$249.1^{+3.1}_{-3.0}$	250.4
$\sqrt{e}\cos\omega$		$0.231^{+0.019}_{-0.020}$	0.230
$\sqrt{e}\sin\omega$		$0.662^{+0.008}_{-0.009}$	0.663
Inclination i	°	$59.3^{+2.3}_{-2.0}$	59.6
PA of asc. node Ω	°	$-12.0^{+4.3}_{-3.9}$	-11.8
Time periastron T_0	BJD	$2455956.7^{+10.7}_{-10.1}$	2455955.1
RV semi-ampl. κ_A	m s^{-1}	$778.7^{+10.5}_{-9.4}$	774.1
Syst. velocity γ	m s^{-1}	$-203.2^{+8.4}_{-8.6}$	-207.4
Parallax π	mas	38.65±0.12	38.66
SMA primary a_1	mas	$16.28^{+0.29}_{-0.26}$	16.12
RV offset ZP$_{\rm SOPHIE}$	m s^{-1}	$90.6^{+15.6}_{-16.9}$	96.2
RV jitter $\sigma_{\rm ELODIE}$	m s^{-1}	$24.4^{+4.1}_{-3.3}$	22.9
RV jitter $\sigma_{\rm SOPHIE}$	m s^{-1}	$16.1^{+5.0}_{-3.5}$	12.67
Computed parameters			
M_1	$M_\odot$	0.99±0.03	1.01
M_2	$M_{\rm J}$	72.4±1.6	72.5
Mass ratio M_2/M_1		0.070±0.002	0.069
Period P	yr	$15.91^{+0.16}_{-0.13}$	15.90
Semi-major axis a	au	$6.45^{+0.08}_{-0.07}$	6.48
Eccentricity e		$0.493^{+0.007}_{-0.008}$	0.493
Arg. periastron ω	°	250.7±1.7	250.9

We note that the proper motion anomaly measured by Hipparcos in RA is different by ∼2σ from the orbital predictions, whereas the measurement in DEC is well reproduced within the uncertainties. The Hipparcos and *Gaia* data affect the derived

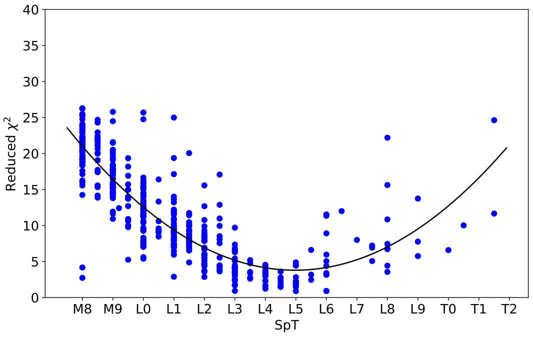

Fig. 3. Reduced χ^2 as a function of the spectral type of the comparison of the IFS spectrum of HD 72946B to SpeX template dwarfs.

orbital parameters and dynamical mass within the uncertainties with respect to a fit that only uses the RV and imaging data, except for breaking the ambiguity in the inclination and longitude of ascending node.

5. Spectral analysis

We used the IRDIS dual-band photometry of the companion to compute the color-magnitude diagram in Appendix D (details from Appendix C of Bonnefoy et al. 2018). We note that HD 72946B is located near mid-L template dwarfs and is close to HIP 65426b (Chauvin et al. 2017).

We compared the IFS spectrum to spectra of template dwarfs of the SpeX spectral library using the SPLAT toolkit (Burgasser 2014). Figure 3 shows the reduced χ^2 as a function of the spectral type. We include the uncertainties of the template spectra in the χ^2 computation. The best-fit object is the red L dwarf 2MASS J03552337+1133437 (Bardalez Gagliuffi et al. 2014) (reduced $\chi^2 = 0.89$, assuming 38 degrees of freedom), which is classified as L5γ by Cruz et al. (2009). From a parabolic fit to the χ^2 values, we estimate a spectral type of L5.0±1.5 considering all spectral types that satisfy $\chi^2 < \chi^2_{\rm min}+1$.

To fit the spectrophotometry of HD 72946B with atmospheric models, we converted the contrast measurements into physical fluxes using a model spectrum for the star ($T_{\rm eff} = 5600$ K, $\log g = 4.5$ dex, and [Fe/H] = 0.0 dex) from the BT-NextGen library (Allard et al. 2012) and the SPHERE filter transmission curves. The BT-NextGen spectrum is fit to the stellar spectral energy distribution (SED) over the range 0.3–12 µm using the Virtual Observatory SED Analyzer (Bayo et al. 2008). The stellar SED is built using data from Tycho (Høg et al. 2000), 2MASS (Cutri et al. 2003), WISE (Cutri & et al. 2013), and IRAS (Helou & Walker 1988), as well as Johnson photometry (Mermilliod 2006) and Strömgren photometry (Paunzen 2015).

We show in Fig. 4 the resulting SED of HD 72946B. We performed a grid search for best-fit models in the BT-Settl spectral library (Allard et al. 2011). The characteristics of the grid are $T_{\rm eff} = 700$–2500 K by steps of 100 K, $\log g = 3.5$–5.5 dex by steps of 0.5 dex, and [Fe/H] = 0.0 dex. We allowed the radius to vary and kept solutions with radii in the range 0.7-1.1 $R_{\rm J}$. We show the four best-match model spectra in Fig. 4. An effective temperature of ∼1700 K provides a good match to the data, which is in the range expected from evolutionary models for an age of ∼1–3 Gyr given the dynamical mass. It also agrees with a spectral type of L5 from the relation for field dwarfs in Filippazzo et al. (2015) (left panel of their Fig. 15).

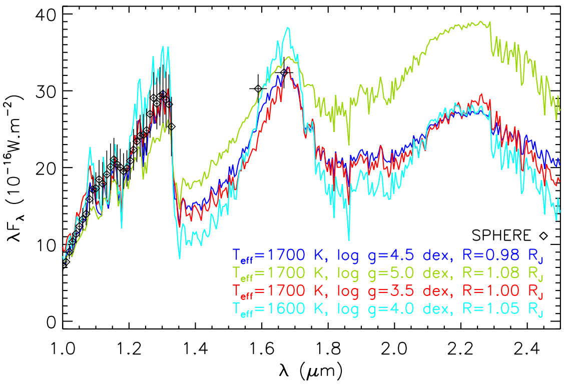

Fig. 4. Spectral energy distribution of HD 72946B (black). The four best-match BT-Settl spectra are shown for comparison (colors).

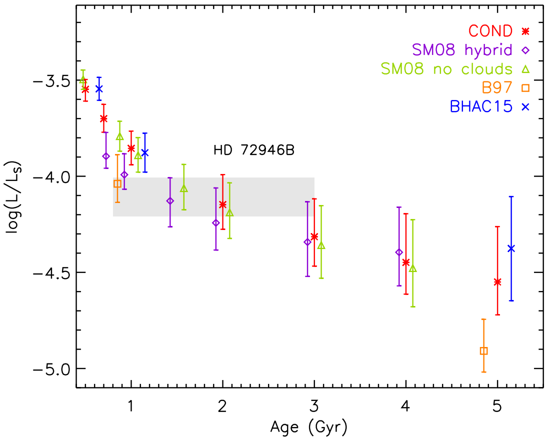

Fig. 5. Bolometric luminosity vs. age of HD 72946B (gray area) compared to evolutionary tracks from the models COND (Baraffe et al. 2003), Saumon & Marley (2008) (for two treatments of the clouds), Burrows et al. (1997), and Baraffe et al. (2015) assuming the mass range for the companion from the orbital fit (data points). Small horizontal offsets are applied to all models except for COND for clarity.

6. Discussion

HD 72946B joins the short list of benchmark brown dwarf companions to stars with RV and imaging measurements: HR 7672B (Liu et al. 2002; Crepp et al. 2012), HD 19467B (Crepp et al. 2014), HD 4747B (Sahlmann et al. 2011; Crepp et al. 2016; Peretti et al. 2018), GJ 758B (Thalmann et al. 2009; Bowler et al. 2018), HD 4113C (Cheetham et al. 2018b), and GJ 229B (Nakajima et al. 1995; Brandt et al. 2019b). HD 72946B stands out among these objects because a complete orbit is covered by RV and it has the smallest physical separation to the star, ∼6.4-6.5 au. This is slightly outside the ice line for a Sun-like star.

To evaluate a possible formation mechanism for HD 72946B, we compared its mass (or mass ratio to the star) and separation to model objects formed by fragmentation of a collapsing cloud in Bate (2009) (Fig. 21) or by disk gravitational instabilities in Forgan & Rice (2013) and Vigan et al. (2017) (left panel of Fig. 8 in the latter paper). The semi-major axes of most of the model objects with mass ratios similar to HD 72946B formed in the former process are in the range 20–5000 au. The semi-major axes of most of the model objects with masses similar to HD 72946B formed in the latter process are in the range ∼10–50 au. This means that the semi-major axis of HD 72946B is smaller than those of model objects from both formation mechanisms, and we cannot exclude any of them.

Figure 5 shows the estimated bolometric luminosity and age of HD 72946B with the predictions from the models COND (Baraffe et al. 2003), Saumon & Marley (2008) (for two treatments of the clouds, hybrid and no clouds), Burrows et al. (1997), and Baraffe et al. (2015) assuming the 95.4% confidence interval for the companion mass from the orbital fit (72.4±3.2 M_J). We estimate the bolometric luminosity to be $\log(L/L_{\odot}) = -4.11 \pm 0.10$ dex using the magnitude-bolometric luminosity relation in Filippazzo et al. (2015) for field dwarfs and the J_s magnitude computed from the IFS spectrum (15.44±0.13 mag) with a correction of 0.05 dex between the J_s and J bands estimated using SpeX spectra of the three best-fit template dwarfs. The J-$H3$ color of the companion (1.08±0.08 mag) is consistent with expectations from mid-L field dwarfs (Cheetham et al. 2019) and is closer to the color predicted given the mass and age of the companion by the DUSTY model (cloudy atmosphere, Chabrier et al. 2000, J-$H3$>1 mag) than to the color predicted by the COND model (cloudless atmosphere, J-$H3$<0.8 mag)[2]. This suggests a cloudy atmosphere. For ages younger than 800 Myr, HD 72946B is fainter than the predictions of all evolutionary models. At 1 Gyr, the companion properties are best reproduced by the hybrid cloud model of Saumon & Marley (2008) and Burrows et al. (1997). At 2 Gyr, the best-match models are COND and the cloudless model of Saumon & Marley (2008), and Baraffe et al. (2015). At 3 Gyr, the models of Baraffe et al. (2015) account better for the companion properties. Observations to better constrain the stellar age with gyrochronology may allow a better distinction between the models.

The characterization of HD 72946B clearly illustrates the improvements in the high-contrast imaging instrumentation toward bridging the gap in separation to the star with RV and astrometry. The combination of these data provides stronger constraints on the properties of substellar companions than can be reached with one technique alone. This allows testing their mass-luminosity models. The SPHERE data are sensitive to low-mass brown dwarfs down to ~30 M_J at separations as close as 0.2″ (Appendix E). The next generation of high-contrast imaging instruments on extremely large telescopes will enable extending analyses like this to the bulk of substellar companions that are detected with RV at closer separations and at lower masses down to the planetary regime and building empirical mass-luminosity relations for exoplanets. The future release of the *Gaia* epoch astrometry will permit more accurate measurements of proper motion anomalies. This will improve dynamical mass estimates and provide new targets for this purpose.

Acknowledgements. The authors thank the referee for a constructive report that helped to clarify the manuscript. The authors thank the ESO Paranal Staff for support in conducting the observations. N.G. and J.O. acknowledge financial support from the ICM (Iniciativa Científica Milenio) via the Núcleo Milenio de Formación Planetaria grant, from the Universidad de Valparaíso, and from Fondecyt (grant 1180395). N. G. acknowledges grant support from project CONICYT-PFCHA/Doctorado Nacional/2017 folio 21170650. We acknowledge financial support from the Programme National de Planétologie (PNP), the Programme National de Physique Stellaire (PNPS) of CNRS-INSU in France, and the Agence Nationale de la Recherche (GIPSE project; grant ANR-14-CE33-0018). T.H. acknowledges support from the European Research Council under the Horizon 2020 Framework Program via the ERC Advanced Grant Origins 83 24 28. This work made use of recipes from the IDL libraries: IDL Astronomy Users's Library (Landsman 1993), Coyote (`http://www.idlcoyote.com/index.html`), EXOFAST (Eastman et al. 2013), JBIU (`http://www.simulated-galaxies.ua.edu/jbiu/`), and the s3drs package (`http://www.heliodocs.com/xdoc/index.html`). It also made use of the Python packages: NumPy (Oliphant 2006), emcee (Foreman-Mackey et al. 2013), corner (Foreman-Mackey 2016), Matplotlib (Hunter 2007), Astropy (Astropy Collaboration et al. 2013, 2018), and dateutil (`http://dateutil.readthedocs.io/`). This publication makes use of VOSA, developed under the Spanish Virtual Observatory project supported by the Spanish MINECO through grant AyA2017-84089. VOSA has been partially updated by using funding from the European Union's Horizon 2020 Research and Innovation Programme, under Grant Agreement n° 776403 (EXOPLANETS-A). This research has benefitted from the SpeX Prism Spectral Libraries, maintained by Adam Burgasser at `http://pono.ucsd.edu/~adam/browndwarfs/spexprism`. This research made use of the SIMBAD database and the VizieR Catalogue access tool, both operated at the CDS, Strasbourg, France. The original descriptions of the SIMBAD and VizieR services were published in Wenger et al. (2000) and Ochsenbein et al. (2000). This research has made use of NASA's Astrophysics Data System Bibliographic Services.

References

Aguilera-Gómez, C., Ramírez, I., & Chanamé, J. 2018, A&A, 614, A55
Allard, F., Homeier, D., & Freytag, B. 2011, in Astronomical Society of the Pacific (ASP) Conf. Ser., ed. C. Johns-Krull, M. K. Browning, & A. A. West, Vol. 448, 91
Allard, F., Homeier, D., Freytag, B., & Sharp, C. M. 2012, in EAS Publications Ser., ed. C. Reylé, C. Charbonnel, & M. Schultheis, Vol. 57, 3–43
Astropy Collaboration, Price-Whelan, A. M., Sipőcz, B. M., et al. 2018, AJ, 156, 123
Astropy Collaboration, Robitaille, T. P., Tollerud, E. J., et al. 2013, A&A, 558, A33
Bailey, V., Meshkat, T., Reiter, M., et al. 2014, ApJL, 780, L4
Baraffe, I., Chabrier, G., Barman, T. S., Allard, F., & Hauschildt, P. H. 2003, A&A, 402, 701
Baraffe, I., Homeier, D., Allard, F., & Chabrier, G. 2015, A&A, 577, A42
Bardalez Gagliuffi, D. C., Burgasser, A. J., Gelino, C. R., et al. 2014, ApJ, 794, 143
Bate, M. R. 2009, MNRAS, 392, 590
Bayo, A., Rodrigo, C., Barrado Y Navascués, D., et al. 2008, A&A, 492, 277
Beichman, C., Gelino, C. R., Kirkpatrick, J. D., et al. 2014, ApJ, 783, 68
Beuzit, J. L., Vigan, A., Mouillet, D., et al. 2019, A&A, 631, A155
Boccaletti, A., Sezestre, E., Lagrange, A.-M., et al. 2018, A&A, 614, A52
Bonnefoy, M., Chauvin, G., Lagrange, A.-M., et al. 2014, A&A, 562, A127
Bonnefoy, M., Perraut, K., Lagrange, A. M., et al. 2018, A&A, 618, A63
Boro Saikia, S., Marvin, C. J., Jeffers, S. V., et al. 2018, A&A, 616, A108
Boss, A. P. 1997, Science, 276, 1836
Bouchy, F., Ségransan, D., Díaz, R. F., et al. 2016, A&A, 585, A46
Bowler, B. P., Dupuy, T. J., Endl, M., et al. 2018, AJ, 155, 159
Brandt, T. D. 2018, ApJS, 239, 31
Brandt, T. D. 2019, ApJS, 241, 39
Brandt, T. D., Dupuy, T. J., & Bowler, B. P. 2019a, AJ, 158, 140
Brandt, T. D., Dupuy, T. J., Bowler, B. P., et al. 2019b, arXiv e-prints, arXiv:1910.01652
Burgasser, A. J. 2014, in Astronomical Society of India Conf. Ser., Vol. 11, 7
Burningham, B., Pinfield, D. J., Leggett, S. K., et al. 2008, MNRAS, 391, 320
Burrows, A., Marley, M., Hubbard, W. B., et al. 1997, ApJ, 491, 856
Cantalloube, F., Mouillet, D., Mugnier, L. M., et al. 2015, A&A, 582, A89
Carbillet, M., Bendjoya, P., Abe, L., et al. 2011, Exp. Astron., 30, 39
Casagrande, L., Schönrich, R., Asplund, M., et al. 2011, A&A, 530, A138
Chabrier, G., Baraffe, I., Allard, F., & Hauschildt, P. 2000, ApJ, 542, 464
Chauvin, G., Desidera, S., Lagrange, A.-M., et al. 2017, A&A, 605, L9
Cheetham, A., Bonnefoy, M., Desidera, S., et al. 2018a, A&A, 615, A160
Cheetham, A., Ségransan, D., Peretti, S., et al. 2018b, A&A, 614, A16
Cheetham, A. C., Samland, M., Brems, S. S., et al. 2019, A&A, 622, A80
Claudi, R. U., Turatto, M., Gratton, R. G., et al. 2008, in SPIE Conf. Ser., Vol. 7014, 70143E
Crepp, J. R., Gonzales, E. J., Bechter, E. B., et al. 2016, ApJ, 831, 136
Crepp, J. R., Johnson, J. A., Fischer, D. A., et al. 2012, ApJ, 751, 97
Crepp, J. R., Johnson, J. A., Howard, A. W., et al. 2014, ApJ, 781, 29
Cruz, K. L., Kirkpatrick, J. D., & Burgasser, A. J. 2009, AJ, 137, 3345
Cutri, R. M. & et al. 2013, VizieR Online Data Catalog, 2328, 0
Cutri, R. M., Skrutskie, M. F., van Dyk, S., et al. 2003, VizieR Online Data Catalog, 2246, 0
da Silva, L., Girardi, L., Pasquini, L., et al. 2006, A&A, 458, 609
De Rosa, R. J., Patience, J., Ward-Duong, K., et al. 2014, MNRAS, 445, 3694
Delorme, P., Delfosse, X., Albert, L., et al. 2008, A&A, 482, 961
Delorme, P., Schmidt, T., Bonnefoy, M., et al. 2017, A&A, 608, A79
Dieterich, S. B., Weinberger, A. J., Boss, A. P., et al. 2018, ApJ, 865, 28
Dohlen, K., Langlois, M., Saisse, M., et al. 2008, in SPIE Conf. Ser., Vol. 7014, 70143L
Dommanget, J. & Nys, O. 2002, VizieR Online Data Catalog, I/274
Ducourant, C., Teixeira, R., Galli, P. A. B., et al. 2014, A&A, 563, A121

---

[2] Tables available at `http://perso.ens-lyon.fr/france.allard/`.

Dupuy, T. J. & Kraus, A. L. 2013, Science, 341, 1492
Dupuy, T. J. & Liu, M. C. 2017, ApJS, 231, 15
Duquennoy, A. & Mayor, M. 1991, A&A, 500, 337
Earl, D. J. & Deem, M. W. 2005, Physical Chemistry Chemical Physics (Incorporating Faraday Transactions), 7, 3910
Eastman, J., Gaudi, B. S., & Agol, E. 2013, PASP, 125, 83
Faherty, J. K., Burgasser, A. J., Walter, F. M., et al. 2012, ApJ, 752, 56
Feroz, F., Balan, S. T., & Hobson, M. P. 2011, Monthly Notices of the Royal Astronomical Society, 416, L104
Filippazzo, J. C., Rice, E. L., Faherty, J., et al. 2015, ApJ, 810, 158
Foreman-Mackey, D. 2016, The Journal of Open Source Software, 1, 24
Foreman-Mackey, D., Hogg, D. W., Lang, D., & Goodman, J. 2013, PASP, 125, 306
Forgan, D. & Rice, K. 2013, MNRAS, 432, 3168
Gaia Collaboration, Brown, A. G. A., Vallenari, A., et al. 2018, A&A, 616, A1
Gaia Collaboration, Prusti, T., de Bruijne, J. H. J., et al. 2016, A&A, 595, A1
Galicher, R., Boccaletti, A., Mesa, D., et al. 2018, A&A, 615, A92
Gauza, B., Béjar, V. J. S., Pérez-Garrido, A., et al. 2015, ApJ, 804, 96
Gizis, J. E., Allers, K. N., Liu, M. C., et al. 2015, ApJ, 799, 203
Goodman, J. & Weare, J. 2010, Communications in Applied Mathematics and Computational Science, 5, 65
Gray, R. O., Corbally, C. J., Garrison, R. F., McFadden, M. T., & Robinson, P. E. 2003, AJ, 126, 2048
Grether, D. & Lineweaver, C. H. 2006, The Astrophysical Journal, 640, 1051
Hayes, D. S. 1985, in IAU Symposium, Vol. 111, Calibration of Fundamental Stellar Quantities, ed. D. S. Hayes, L. E. Pasinetti, & A. G. D. Philip, 225–252
Helou, G. & Walker, D. W., eds. 1988, Infrared astronomical satellite (IRAS) catalogs and atlases. Volume 7: The small scale structure catalog, Vol. 7
Høg, E., Fabricius, C., Makarov, V. V., et al. 2000, A&A, 355, L27
Hunter, J. D. 2007, Computing in Science & Engineering, 9, 90
Kirkpatrick, J. D., Cushing, M. C., Gelino, C. R., et al. 2011, ApJS, 197, 19
Kirkpatrick, J. D., Gelino, C. R., Cushing, M. C., et al. 2012, ApJ, 753, 156
Kirkpatrick, J. D., Reid, I. N., Liebert, J., et al. 2000, AJ, 120, 447
Konopacky, Q. M., Ghez, A. M., Barman, T. S., et al. 2010, ApJ, 711, 1087
Konopacky, Q. M., Thomas, S. J., Macintosh, B. A., et al. 2014, in Society of Photo-Optical Instrumentation Engineers (SPIE) Conference Series, Vol. 9147, Ground-based and Airborne Instrumentation for Astronomy V, 914784
Lachapelle, F.-R., Lafrenière, D., Gagné, J., et al. 2015, ApJ, 802, 61
Lafrenière, D., Jayawardhana, R., & van Kerkwijk, M. H. 2010, ApJ, 719, 497
Landsman, W. B. 1993, in Astronomical Society of the Pacific Conference Series, Vol. 52, Astronomical Data Analysis Software and Systems II, ed. R. J. Hanisch, R. J. V. Brissenden, & J. Barnes, 246
Langlois, M., Vigan, A., Moutou, C., et al. 2013, in Proceedings of the Third AO4ELT Conference, ed. S. Esposito & L. Fini, 63
Leggett, S. K., Allard, F., Dahn, C., et al. 2000, ApJ, 535, 965
Lindegren, L., Hernández, J., Bombrun, A., et al. 2018, A&A, 616, A2
Liu, M. C., Dupuy, T. J., & Allers, K. N. 2016, ApJ, 833, 96
Liu, M. C., Fischer, D. A., Graham, J. R., et al. 2002, ApJ, 571, 519
Liu, M. C., Magnier, E. A., Deacon, N. R., et al. 2013, ApJ, 777, L20
Lucas, P. W., Tinney, C. G., Burningham, B., et al. 2010, MNRAS, 408, L56
Luck, R. E. 2017, AJ, 153, 21
Luck, R. E. & Heiter, U. 2006, AJ, 131, 3069
Luhman, K. L. & Esplin, T. L. 2016, AJ, 152, 78
Ma, B. & Ge, J. 2014, Monthly Notices of the Royal Astronomical Society, 439, 2781
Mace, G. N., Kirkpatrick, J. D., Cushing, M. C., et al. 2013, ApJS, 205, 6
Macintosh, B., Graham, J. R., Ingraham, P., et al. 2014, PNAS, 111, 12661
Maire, A.-L., Langlois, M., Dohlen, K., et al. 2016, in SPIE Conf. Ser., Vol. 9908, 990834
Maire, A.-L., Skemer, A. J., Hinz, P. M., et al. 2015, A&A, 576, A133
Makarov, V. V. & Kaplan, G. H. 2005, AJ, 129, 2420
Mamajek, E. E. & Hillenbrand, L. A. 2008, ApJ, 687, 1264
Marois, C., Correia, C., Galicher, R., et al. 2014, in SPIE Conf. Ser., Vol. 9148, 91480U
Marois, C., Lafrenière, D., Doyon, R., Macintosh, B., & Nadeau, D. 2006, ApJ, 641, 556
Martinez, P., Dorrer, C., Aller Carpentier, E., et al. 2009, A&A, 495, 363
Martínez-Arnáiz, R., Maldonado, J., Montes, D., Eiroa, C., & Montesinos, B. 2010, A&A, 520, A79
Mawet, D., Milli, J., Wahhaj, Z., et al. 2014, ApJ, 792, 97
Mermilliod, J. C. 2006, VizieR Online Data Catalog, II/168
Mesa, D., Gratton, R., Zurlo, A., et al. 2015, A&A, 576, A121
Montes, D., López-Santiago, J., Gálvez, M. C., et al. 2001, MNRAS, 328, 45
Mountain, C. M., Leggett, S. K., Selby, M. J., Blackwell, D. E., & Petford, A. D. 1985, A&A, 151, 399
Mugnier, L. M., Cornia, A., Sauvage, J.-F., et al. 2009, Journal of the Optical Society of America A, 26, 1326
Nakajima, T., Oppenheimer, B. R., Kulkarni, S. R., et al. 1995, Nature, 378, 463
Nielsen, E. L., De Rosa, R. J., Macintosh, B., et al. 2019, AJ, 158, 13
Ochsenbein, F., Bauer, P., & Marcout, J. 2000, A&AS, 143, 23
Oh, S., Price-Whelan, A. M., Hogg, D. W., Morton, T. D., & Spergel, D. N. 2017, AJ, 153, 257
Oliphant, T. E. 2006, A guide to NumPy, Vol. 1 (Trelgol Publishing USA)
Patience, J., King, R. R., de Rosa, R. J., & Marois, C. 2010, A&A, 517, A76
Paunzen, E. 2015, A&A, 580, A23
Pavlov, A., Möller-Nilsson, O., Feldt, M., et al. 2008, in SPIE Conf. Ser., Vol. 7019, 701939
Peretti, S., Ségransan, D., Lavie, B., et al. 2018, A&A, in press, arXiv:1805.05645
Perrin, M. D., Ingraham, P., Follette, K. B., et al. 2016, in Society of Photo-Optical Instrumentation Engineers (SPIE) Conference Series, Vol. 9908, Ground-based and Airborne Instrumentation for Astronomy VI, 990837
Perrin, M. D., Maire, J., Ingraham, P., et al. 2014, in SPIE Conf. Ser., Vol. 9147, 3
Perryman, M. A. C., Lindegren, L., Kovalevsky, J., et al. 1997, A&A, 500, 501
Pourbaix, D., Tokovinin, A. A., Batten, A. H., et al. 2004, A&A, 424, 727
Rajan, A., Rameau, J., De Rosa, R. J., et al. 2017, AJ, 154, 10
Ramírez, I., Fish, J. R., Lambert, D. L., & Allende Prieto, C. 2012, ApJ, 756, 46
Rocha-Pinto, H. J., Flynn, C., Scalo, J., et al. 2004, A&A, 423, 517
Sahlmann, J., Ségransan, D., Queloz, D., et al. 2011, Astronomy and Astrophysics, 525, A95
Saumon, D. & Marley, M. S. 2008, ApJ, 689, 1327
Schlieder, J. E., Skemer, A. J., Maire, A.-L., et al. 2016, ApJ, 818, 1
Schneider, A. C., Cushing, M. C., Kirkpatrick, J. D., et al. 2015, ApJ, 804, 92
Sestito, P., Randich, S., & Pallavicini, R. 2004, A&A, 426, 809
Soummer, R., Pueyo, L., & Larkin, J. 2012, ApJL, 755, L28
Stone, J. M., Skemer, A. J., Kratter, K. M., et al. 2016, ApJ, 818, L12
Thalmann, C., Carson, J., Janson, M., et al. 2009, ApJL, 707, 123
Tinney, C. G., Faherty, J. K., Kirkpatrick, J. D., et al. 2014, ApJ, 796, 39
van Leeuwen, F. 2007, A&A, 474, 653
Vigan, A., Bonavita, M., Biller, B., et al. 2017, A&A, 603, A3
Vigan, A., Gry, C., Salter, G., et al. 2015, MNRAS, 454, 129
Vigan, A., Moutou, C., Langlois, M., et al. 2010, MNRAS, 407, 71
Wahhaj, Z., Liu, M. C., Biller, B. A., et al. 2011, ApJ, 729, 139
Warren, S. J., Mortlock, D. J., Leggett, S. K., et al. 2007, MNRAS, 381, 1400
Wenger, M., Ochsenbein, F., Egret, D., et al. 2000, A&AS, 143, 9
Zapatero Osorio, M. R., Béjar, V. J. S., Miles-Páez, P. A., et al. 2014, A&A, 568, A6

---

[1] STAR Institute, Université de Liège, Allée du Six Août 19c, B-4000 Liège, Belgium
e-mail: `almaire@uliege.be`
[2] Department of Physics, University of Oxford, Oxford, UK
[3] INAF–Osservatorio Astronomico di Padova, Vicolo dell'Osservatorio 5, I-35122 Padova, Italy
[4] INAF Catania Astrophysical Observatory, via S. Sofia 78, 95123 Catania, Italy
[5] Max-Planck-Institut für Astronomie, Königstuhl 17, D-69117 Heidelberg, Germany
[6] Instituto de Física y Astronomía, Facultad de Ciencias, Univ. de Valparaíso, Av. Gran Bretaña 1111, Playa Ancha, Valparaíso, Chile
[7] Núcleo Milenio Formación Planetaria - NPF, Univ. de Valparaíso, Av. Gran Bretaña 1111, Playa Ancha, Valparaíso, Chile
[8] LESIA, Observatoire de Paris, PSL Research University, CNRS, Sorbonne Universités, UPMC Univ. Paris 06, Univ. Paris Diderot, Sorbonne Paris Cité, 5 place Jules Janssen, F-92195 Meudon, France
[9] Univ. Grenoble Alpes, CNRS, IPAG, F-38000 Grenoble, France
[10] Geneva Observatory, University of Geneva, Chemin des Maillettes 51, 1290 Versoix, Switzerland
[11] Unidad Mixta Internacional Franco-Chilena de Astronomía CNRS/INSU UMI 3386 and Departamento de Astronomía, Universidad de Chile, Casilla 36-D, Santiago, Chile
[12] CRAL, UMR 5574, CNRS/ENS-Lyon/Université Lyon 1, 9 av. Ch. André, F-69561 Saint-Genis-Laval, France

Appendix A: Stellar multiplicity

Bouchy et al. (2016) noted that HD 72946 is part of a multiple system. HD 72945 is a comoving F8 star located at a projected separation of 230 au. Duquennoy & Mayor (1991) identified it as a spectroscopic binary SB1 with a period of 14.3 d.

The Gaia parallaxes of HD 72945 and HD 72946 differ at the 4.2σ level, indicating a distance difference along the line of sight of about 0.41±0.10 pc. The similar proper motion and systematic velocities of the two stars argue in favor of a physical association (see also Oh et al. 2017). We speculate that the separation along the line of sight could be significantly larger than the one projected on the plane of the sky. Alternatively, the parallaxes of one or both components can be altered above the formal errors by the presence of the companions.

In addition, Dommanget & Nys (2002) reported three stellar companions with angular separations of 93″, 117″, and 122″.

Using the *Gaia* parallaxes, we find that the three components identified by Dommanget & Nys (2002) ($\pi < 12$ mas) do not form a system with HD 72945 and HD 72946 ($\pi \sim 38$–39 mas). Instead, we note in the *Gaia* catalog a star (2MASS ID 08354678+0635294) at ~130″ (~3400 au) from HD 72946 with a parallax of 38.8196±0.0584 mas (distance along the line of sight ~0.11±0.05 pc) and similar proper motion, but without a measured RV. Therefore we argue that the system is formed by four stellar and one substellar components. For the orbital analysis, we assumed that the acceleration seen in the proper motion of HD 72946 is entirely due to the substellar companion HD 72946B.

The other components may provide additional constraints on the age of the system. In particular, we derive for HD 72945 an age and a mass using the PARAM web interface, the $T_{\rm eff}$ derived by Casagrande et al. (2011) from Strömgren photometry, the *Gaia* parallax, the V magnitude from Hipparcos (5.92±0.01 mag), and the metallicity measured by Bouchy et al. (2016) for HD 72946 (0.01-dex difference only with the metallicity of HD 72945 measured by Casagrande et al. 2011). We find an age of 1.584±0.952 Gyr and a mass of 1.245±0.030 $M_\odot$. For this computation, we assumed that the spectroscopic companion of HD 72945 does not contribute significantly to the integrated photometry. This should be the case if its mass is not much higher than the expected minimum mass from the RV orbit. Using the SB9 orbit (Pourbaix et al. 2004) and the isochronal mass above, we derive a minimum mass for the secondary of 0.34 $M_\odot$. In any case, a significant contribution to the photometry would shift the measured isochronal age toward higher values than expected. We report archival GPI data of HD 72945 in Appendix F.

Appendix B: Comparison of extracted spectrophotometry

We show in Fig. B.1 the comparison of the spectrophotometry extracted with the ANgular DiffeRential Optimal Method Exoplanet Detection Algorithm (ANDROMEDA, Mugnier et al. 2009; Cantalloube et al. 2015) and with the Template Locally Optimized Combination of Images (TLOCI, Marois et al. 2014) and Principal Component Analysis (PCA, Soummer et al. 2012) algorithms provided by the SpeCal pipeline (Galicher et al. 2018). For the TLOCI extraction, we used the fitting of a model planet image, whereas for PCA we employed the negative synthetic planet injection. The fitting uncertainties are given at 3 σ. We note the good agreement between the TLOCI and PCA results within the TLOCI uncertainties. The IFS spectra between TLOCI and ANDROMEDA did not formerly agree for wavelengths longer than ~1.2 µm, with the ANDROMEDA spectrum showing a steeper slope than the TLOCI spectrum. The IRDIS photometry for ANDROMEDA looks fainter than the TLOCI photometry by ~15%, although the uncertainties are large. This results in an IRDIFS spectrum that is redder for TLOCI than for ANDROMEDA.

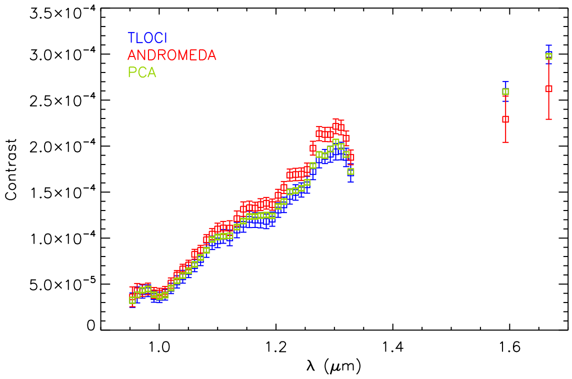

Fig. B.1. Comparison of the TLOCI, ANDROMEDA, and PCA spectrophotometry. The measurement uncertainties are shown at 3 σ for all algorithms.

We tested both ANDROMEDA and TLOCI SED for the atmospheric fitting. We experienced convergence problems when fitting the ANDROMEDA SED, and we chose the TLOCI SED for the analysis shown in this paper. We did not notice any significant discrepancies in the extracted astrometry, but we chose to use the TLOCI astrometry for consistency.

Appendix C: Corner plot of the orbital fit

We provide here the corner plot of the orbital parameters derived in Sect. 4.

Appendix D: Color-magnitude diagram

To build the diagram in Fig. D.1, we used spectra of M, L, and T dwarfs from the SpeX-Prism library (Burgasser 2014) and from Leggett et al. (2000) and Schneider et al. (2015) to generate synthetic photometry in the SPHERE filter passbands. The zero-points were computed using a flux-calibrated spectrum of Vega (Hayes 1985; Mountain et al. 1985). We also considered the spectra of young and/or dusty free-floating objects from Liu et al. (2013), Mace et al. (2013), Gizis et al. (2015), and of young companions (Wahhaj et al. 2011; Gauza et al. 2015; Stone et al. 2016; De Rosa et al. 2014; Lachapelle et al. 2015; Bailey et al. 2014; Rajan et al. 2017; Bonnefoy et al. 2014; Patience et al. 2010; Lafrenière et al. 2010; Chauvin et al. 2017; Delorme et al. 2017; Cheetham et al. 2018a). The colors and absolute fluxes of the benchmark companions and isolated T-type objects were generated from the distance and spectra of these objects in Appendix B in Bonnefoy et al. (2018). To conclude, we used the spectra of Y dwarfs published in Schneider et al. (2015), Warren et al. (2007), Delorme et al. (2008), Burningham et al. (2008), Lucas et al. (2010), Kirkpatrick et al. (2012), and Mace et al. (2013) to extend the diagrams in the late-T and early-Y dwarf domain. We used the distances of the field dwarfs reported in Kirkpatrick et al. (2000), Faherty et al. (2012), Dupuy & Kraus (2013), Tinney et al. (2014), Beichman et al. (2014),

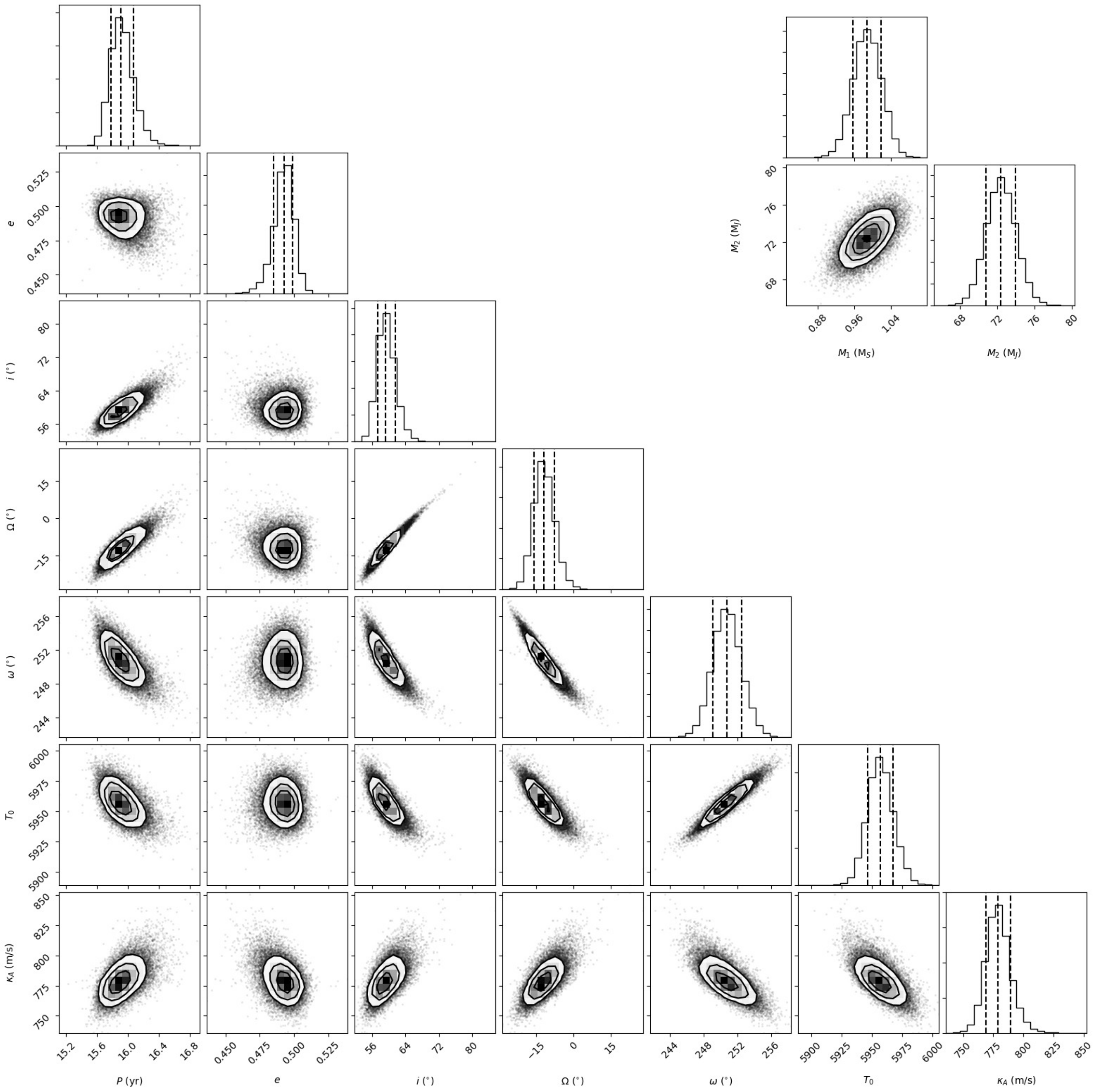

Fig. C.1. MCMC posteriors of the orbital parameters (*left*) and of the masses of HD 72946 A and B (*top right*). The diagrams displayed on the diagonals represent the 1D histogram distributions for the parameters. The off-diagonal diagrams show the correlations. In the histograms, the dashed vertical lines indicate the 16%, 50%, and 84% quantiles.

and Luhman & Esplin (2016). We considered those reported in Kirkpatrick et al. (2011), Faherty et al. (2012), Zapatero Osorio et al. (2014), and Liu et al. (2016) for the dusty dwarfs. The companion distances were taken from van Leeuwen (2007) and Ducourant et al. (2014).

Appendix E: SPHERE detection limits

Figure E.1 shows the SPHERE detection limits in contrast to the star and the planet mass obtained with ANDROMEDA. For the IFS detection limits, we assumed a T5 dwarf template spectrum (Cantalloube et al., in preparation) retrieved from the SpeX library. The detection limits account for the coronagraphic transmission (Boccaletti et al. 2018) and the small sample statistics correction (Mawet et al. 2014). The contrast to planet mass conversion was derived assuming the "hot-start" evolutionary and atmospheric models of Baraffe et al. (2003, 2015) and an age of 2 Gyr for the system (table from Vigan et al. 2015). The H3 curve is sensitive to more massive objects than the H2 curve because the probed mass regime corresponds to cold objects with strong methane absorption features and the H3 filter matches a strong methane band. We excluded additional brown dwarf companions more massive than ~20 M_J at separations beyond 8 au.

Appendix F: GPI archival data of HD 72945

The stellar SB companion HD 72945 was observed with the Gemini Planet Imager (GPI, Macintosh et al. 2014) on 2015

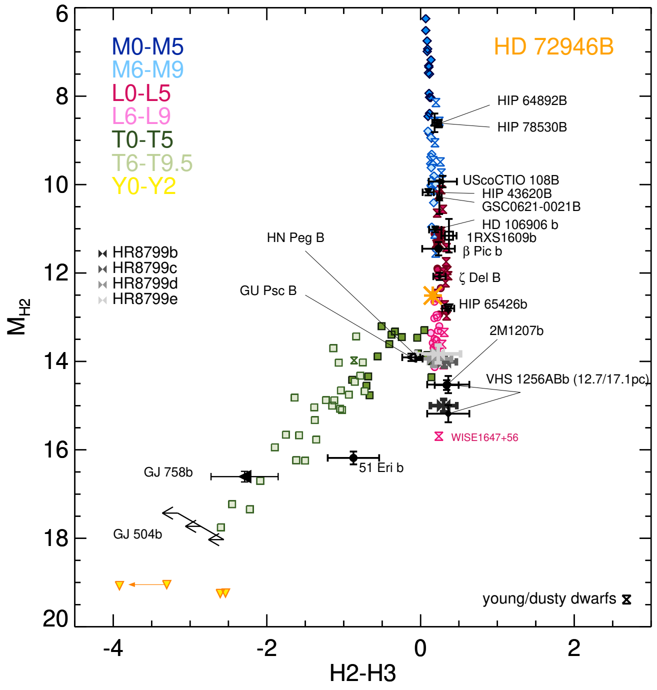

Fig. D.1. Color-magnitude diagram of HD 72946B (orange) using the IRDIS photometry. Template dwarfs (colored points) and a few young low-mass companions (black labels) are also shown for comparison.

April 4 UT in the *H* band. The data were presented in the first statistical analysis of the GPIES survey (Nielsen et al. 2019, target name: HR 3395). The target was observed for an integration time of 32.8 min, which amounts to a field rotation of 19.5°.

We retrieved the data from the Gemini archive and reduced them with the GPI data reduction pipeline v1.4.0 (Perrin et al. 2014, 2016), which applies an automatic correction for the North offset of $-1.00\pm0.03°$ measured by Konopacky et al. (2014). Then, we post-processed them using ANDROMEDA. No point source is detected above 5σ. We show in Fig. F.1 the detection limits obtained for a T5 dwarf template spectrum. We assumed an age of 2 Gyr, a distance of 26.3 pc from the *Gaia* DR2 parallax, and the models of Baraffe et al. (2003, 2015). For the stellar magnitude, we used the 2MASS value, although we note that it is affected by saturation. We included the small sample statistics correction. We cut the curves to separation larger than 0.15″ because we were unable to find GPI coronagraphic transmission curves.

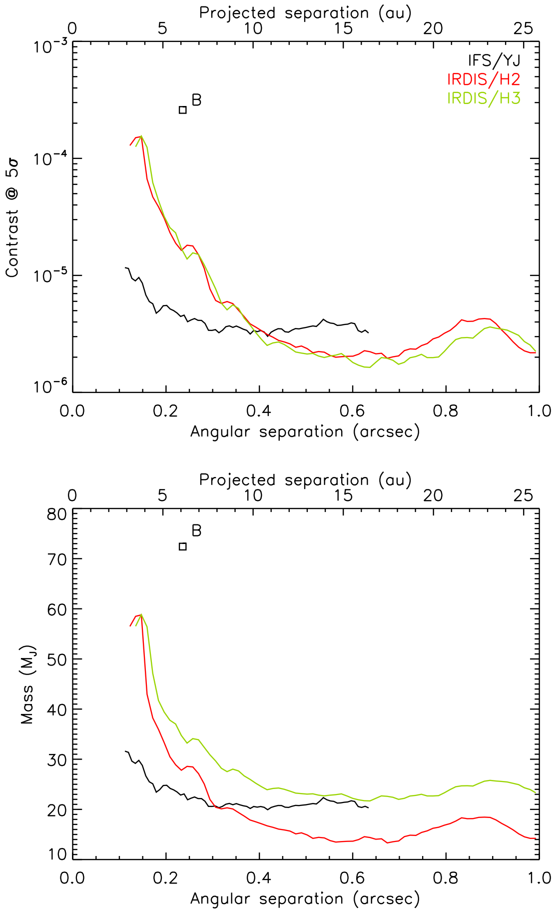

Fig. E.1. SPHERE 5σ detection limits in contrast with respect to the star (*top*) and the planet mass (*bottom*). We also indicate the location of HD 72946B for comparison.

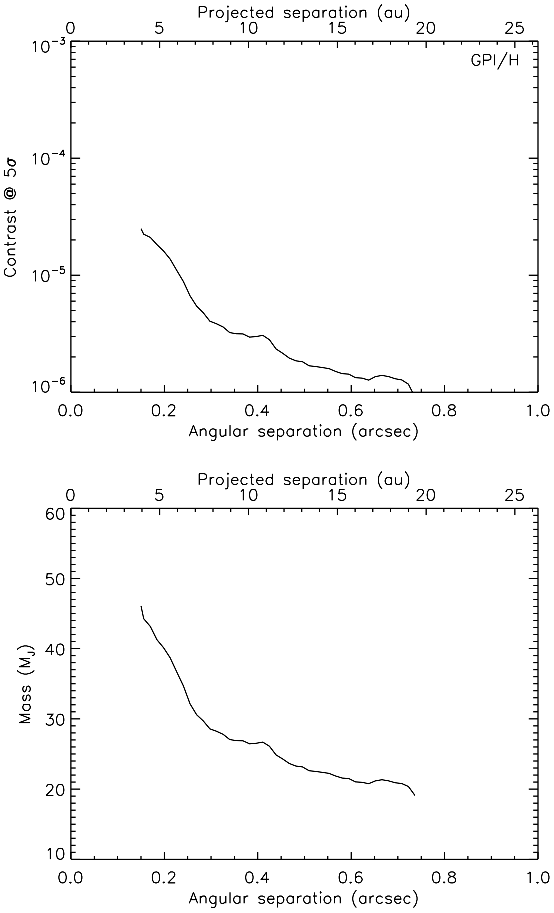

Fig. F.1. GPI 5σ detection limits of HD 72945 in contrast with respect to the star (*top*) and the planet mass (*bottom*).